since 1961

Baltica

BALTICA Volume 32 Number 1 June 2019: 78–90
https://doi.org/10.5200/baltica.2019.1.7

Modelling of glacially-induced stress changes in Latvia, Lithuania and the Kaliningrad District of Russia

Holger Steffen, Rebekka Steffen and Lev Tarasov

Steffen, H., Steffen R., Tarasov L. 2019. Modelling of glacially-induced stress changes in Latvia, Lithuania and the Kaliningrad District of Russia. *Baltica, 32 (1),* 78–90. Vilnius, ISSN 0067-3064.

Manuscript submitted 08 February 2019 / Accepted 20 May 2019 / Published online 20 June 2019

Abstract. We model the change of Coulomb Failure Stress (δCFS) during the Weichselian glaciation up until today at 12 locations in Latvia, Lithuania and Russia that are characterised by soft-sediment deformation structures (SSDS). If interpreted as seismites, these SSDS may point to glacially-induced fault reactivation. The δCFS suggests a high potential of such reactivation when it reaches the instability zone. We show that δCFS at all 12 locations reached this zone several times in the last 120,000 years. Most notably, all locations exhibit the possibility of reactivation after ca. 15 ka BP until today. Another time of possible activity likely happened after the Saalian glaciation until ca. 96 ka BP. In addition, some models suggest unstable states after 96 ka BP until ca. 28 ka BP at selected locations but with much lower positive δCFS values than during the other two periods. For the Valmiera and Rakuti seismites in Latvia, we can suggest a glacially-induced origin, whereas we cannot exactly match the timing at Rakuti. Given the (preliminary) dating of SSDS at some locations, at Dyburiai and Ryadino our modelling supports the interpretation of glacially-induced fault reactivation, while at Slinkis, Kumečiai and Liciškėnai they likely exclude such a source. Overall, the mutual benefit of geological and modelling investigations is demonstrated. This helps in identifying glacially-induced fault reactivation at the south-eastern edge of the Weichselian glaciation and in improving models of glacial isostatic adjustment.

Keywords: *Glacial Isostatic Adjustment; Earthquake; Coulomb Failure Stress; Finite element modelling; Baltic countries; Soft-sediment deformation structure; Seismites*

✉ *Holger Steffen (holger.steffen@lm.se) Geodetic Infrastructure, Lantmäteriet, Lantmäterigatan 2C, 80182 Gävle, Sweden; Rebekka Steffen (rebekka.steffen@lm.se) Geodetic Infrastructure, Lantmäteriet, Lantmäterigatan 2C, 80182 Gävle, Sweden; Lev Tarasov (lev@mun.ca) Department of Physics and Physical Oceanography, Memorial University of Newfoundland, St. John's, NL, A1B 3X7, Canada*

INTRODUCTION

Repeated glaciations during the Pleistocene (2,588.0 to 11.7 thousand years before present (ka BP), Cohen *et al*. 2013 updated) have fundamentally shaped the surface of the Earth, especially due to the development and advance of large continental-scale ice sheets. The interaction of ice sheets with the solid Earth is summarised in the term glacial isostatic adjustment (GIA) and recognises several strongly tied processes (Whitehouse 2018). They include, among others, surface deformation as well as changes in the gravitational potential field, rotation, and stress field of the Earth (Steffen, Wu 2011). Ice sheets also removed water from the oceans so that mean sea level during the Last Glacial Maximum (LGM) was ca. 130–134 m lower than today (Lambeck *et al.* 2014; Peltier *et al.* 2015).

We focus herein on changes in the stress field and their consequences. The weight of an ice sheet bends the lithosphere and induces additional stresses to e.g., lithostatic pressure-induced and tectonic background stresses, in both the vertical and horizontal stress components. We use the term GIA stresses (Steffen *et*

al. 2014b) for these additional stresses. The vertical GIA stresses vanish when the ice melted completely but due to the visco-elastic nature of the Earth's mantle the lithosphere is still deformed and readjusts only slowly towards isostatic equilibrium (Steffen *et al.* 2014a). Therefore, horizontal GIA stresses remain but can be released in earthquakes along pre-existing faults (Steffen *et al.* 2014a). This is evidenced, for example, in northern Fennoscandia in more than a dozen fault scarps of up to 30 m height (Mikko *et al.* 2015). Such faults are known as postglacial faults but are nowadays termed glacially-induced faults (GIF) (Lund 2015). Next to northern Fennoscandia, there is also evidence of such faults and traces of glacially-triggered earthquakes in Denmark, northern Germany, Poland and the United Kingdom (Sandersen, Jørgensen 2015; Brandes *et al.* 2018; Brandes *et al.* 2012; Grube 2019; Hoffmann, Reicherter 2012; Pisarska-Jamroży *et al.* 2018; van Loon, Pisarska-Jamroży 2014; Stewart *et al.* 2001) as well as in North America (Fenton 1994). GIFs are found not only in the centre of former ice sheet locations but also at their margins and beyond (Brandes *et al.* 2012, 2015; Druzhinina *et al.* 2017; Sandersen, Jørgensen 2015; Stewart *et al.* 2000).

A few studies (e.g. Bitinas, Lazauskienė 2011; van Loon *et al.* 2016; Pisarska-Jamroży, Bitinas 2018; Pisarska-Jamroży *et al.* this issue) discuss GIFs or glacially-triggered seismicity in the Baltic area, which represents the south-eastern corner of the Scandinavian Ice Sheet (SIS) during the Weichselian glaciation (ca. 115.0 to 11.7 ka BP), the last of past north-European glaciations. Many tectonic faults have been identified in the crystalline basement of this area (Fig. 1). In view of the modelling results by Brandes *et al*. (2012, 2015, 2018) for central Europe (the south-western corner of the SIS), it is reasonable to assume that GIFs also developed in the countries of Latvia, Lithuania and Russia (Kaliningrad District), as has already been suggested by Bitinas, Lazauskienė (2011). This view is supported by prominent earthquakes in the East Baltic area in historic and recent times (Ņikuļins 2011; Pačėsa, Šliaupa 2011) such as the 1616 earthquake in Latvia (Doss 1910) and the 2004 Kaliningrad earthquake (Ulomov *et al.* 2008). These could be connected to the past glaciation in the same way as Brandes *et al*. (2015) and Brandes *et al*. (2019) suggested for historic and recent earthquakes in Germany.

In the Baltic countries and the Kaliningrad District of Russia, seismic activity is proposed for a dozen locations discussed in the recent literature (Fig. 1). These locations are mostly characterized by soft-sediment deformation structures (SSDS) (see Fig. 2, for example) that, if interpreted as seismites, may point to glacially-triggered seismicity in the near-field of potentially reactivated faults (Fig. 1, Table 1). At some locations the trigger remains unclear. For other locations, triggers such as collapse of river walls are more likely to have generated seismites-like SSDS (e.g. at the Liciškėnai outcrop, see Table 1).

The aims of our study are therefore: (i) to analyse modelled GIA stress changes in view of their poten-

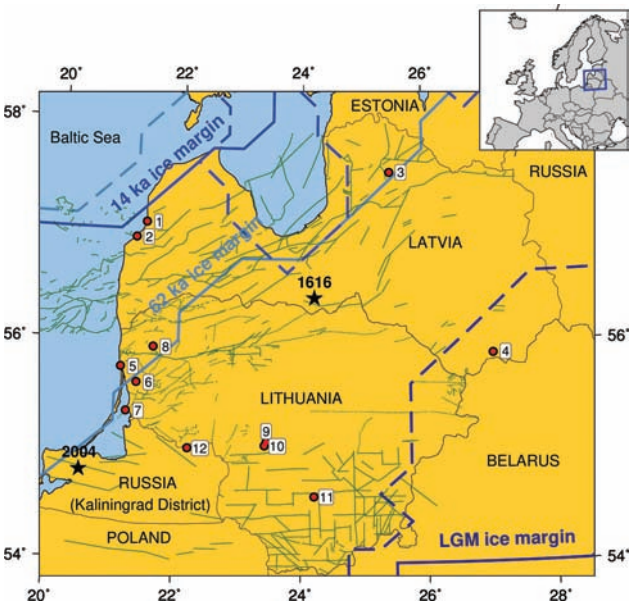

Fig. 1 Geographical overview of locations (red dots) with soft-sediment deformation structures (1–4, 6–12) in Latvia and Lithuania and the Giruliai mega-landslide (5). See Table 1 for location names. Dark green lines: Tectonic faults in the Caledonian structural complex after Ņikuļins (2011, 2019) for Latvia, updated after Čyžienė *et al*. (2007) for Lithuania and after Sharov *et al.* (2007) for Poland and the Kaliningrad District. Black stars: epicentres of the 1616 Latvia and 2004 Kaliningrad earthquakes. Bluish lines represent ice limits from models of the Weichselian glaciation, whereas solid is model ANU-ICE (Lambeck *et al.* 2010) and dashed is model GLAC (Tarasov 2013). Dark blue is limit at Last Glacial Maximum (LGM), common blue at 14 ka, and light blue at 62 ka

Fig. 2 Example of soft-sediment deformation structures in sedimentary unit B at the Slinkis outcrop (#9 in Fig. 1), see also Pisarska-Jamroży *et al.* (this issue) (Photo: Holger Steffen)

Table 1 Overview of locations with known or assumed glacially-induced seismicity in Latvia, Lithuania and the Kaliningrad District of Russia. See Fig. 1 for geographical distribution. Lat. = Latitude, Long. = Longitude, SSDS = Soft-sediment deformation structures

Location	# in Fig. 1	Lat./Long.	Brief description	Timing information	Reference
Sārnate outcrop, Latvia	1	57.07 N 21.42 E	Lake or lagoon environment. SSDS in two units with hiatus, likely one single event, palaeoseismic event possible	Ice-free ca. 14.0 ka, age of organic deposits 7.73 ka and younger	Nartišs *et al.* (2018)
Baltmuiža site, Latvia	2	56.93 N 21.26 E	Lacustrine sediments with 3 SSDS horizons, palaeoseismic event possible	Deposition 28.6–23.4 ka, ice-free ca. 14.0 ka	Belzyt *et al.* (2018a)
Valmiera section, Latvia	3	57.55 N 25.44 E	Glaciofluvial sediments, palaeoseismic event very likely	Deposition <14.5 ka	Van Loon *et al.* (2016)
Rakuti section, Latvia	4	55.90 N 27.09 E	Glaciolacustrine sediments, palaeoseismic event very likely	Deposition 17.0–16.0 ka	Van Loon *et al.* (2016)
Giruliai mega-landslide, Lithuania	5	55.75 N 21.09 E	360 m long mega-landslide, hypothetically triggered by earthquake	Happened 7.7 ka or any time thereafter	Damušytė, Bitinas (2018), Bitinas *et al.* (2016)
Juodikiai quarry, Lithuania	6	55.61 N 21.35 E	Glaciofluvial delta with SSDS, not further investigated	Not available (Late Weichselian)	Bitinas, Damušytė (2018)
Ventės Ragas outcrop, Lithuania	7	55.35 N 21.20 E	Sandy lacustrine and aeolian sediments with SSDS, not further investigated	Not available (Late Weichselian)	Bitinas, Damušytė (2018)
Dyburiai outcrop, Lithuania	8	55.94 N 21.60 E	Glaciolacustrine inter-moraine sediments, palaeoseismic event very likely	Deposition 119.7–91.1 ka, ages subject to debate	Pisarska-Jamroży *et al.* (2018b)
Slinkis outcrop, Lithuania	9	55.09 N 23.45 E	Meandering fluvial system sediments with trapped SSDS, palaeoseismic event or glacial earthquake suggested	Deposition 24.0–21.2 ka	Belzyt *et al.* (2018b), Pisarska-Jamroży *et al.* (this issue)
Kumečiai outcrop, Lithuania	10	55.06 N 23.42 E	Fluvial meandering system sediments with several layers of SSDS, palaeoseismic event unlikely	Deposition 76.0–46.7 ka, ages subject to debate	Pisarska-Jamroży *et al.* (2018c)
Liciškėnai outcrop, Lithuania	11	54.60 N 24.21 E	Glaciolacustrine sediments with SSDS, palaeoseismic event unlikely	Deposition 74.2–51.7 ka, ages subject to debate	Woronko *et al.* (2018)
Ryadino archaeological excavation, Russia	12	55.03 N 22.20 E	Glaciolacustrine sediments with SSDS, palaeoseismic event likely	Deposition 8.7–7.5 ka	Druzhinina *et al.* (2017)

tial to reactivate pre-existing faults in the vicinity of these 12 locations in Latvia, Lithuania and the Kaliningrad District of Russia, and (ii) to provide reasoning for each location if the structures developed due to glacially-triggered seismicity or not. We use Finite Element (FE) models of GIA to calculate the change in Coulomb Failure Stress (δCFS) for each location. We introduce our modelling approach in the next section. This is followed by a presentation of the results and their discussion.

MODELLING

In general, a GIA model consists of an earth model characterized by its specific rheology as well as an ice load history (Whitehouse 2018). Both parts affect the results and their fit to observations and thus there is still no consensus on the best GIA model for the whole of Fennoscandia (Steffen, Wu 2011). Many different ice-earth model combinations give reasonable fits to selected observational datasets and are thus advocated by respective groups (e.g., Lambeck *et al.* 2010; Peltier *et al.* 2015). We test several of such combinations that are discussed for our investigation area to show the spread of possible results so that the reader can get a feeling for the uncertainty of the modelling.

We apply the FE software ABAQUS (ABAQUS 2018) to create a three-dimensional model of the lithosphere and mantle in Fennoscandia. We follow the flat-Earth approach outlined in Wu (1992, 2004) and Steffen *et al.* (2006), which has been shown to agree well with previous numerical solutions of GIA (Wu, Johnston 1998; Spada *et al.* 2011). The model consists of a centre of 4500 km × 4500 km size and a frame that extends the model horizontally to a size of 60,000 km × 60,000 km. This allows mantle material to flow outside the central area and minimize associated numerical errors (Steffen *et al.* 2006). The model reaches the core-mantle boundary at 2891 km depth (Table 2) which has been shown to be appropriate when working with continental-scale ice sheets (Steffen *et al.* 2015). The centre has 90 × 90 hexahedral elements of 50 km × 50 km extent in the horizontals, while the elements of the frame are variable in size, but side length increases from the centre to the edge. The sides of the model are fixed with rigid boundary conditions.

The lithosphere is composed of model-dependent (due to lithospheric thickness) 8 or 9 element layers with the first 6 layers having 5 km thickness each. It represents an elastically behaving outer shell of the Earth whose thickness corresponds to loading processes such as GIA of time-scales of some 1000s to 100,000 years and should therefore not be confused with seismically or geologically derived lithospheric thicknesses (Eaton *et al*. 2009). The upper mantle down to 670 km has 4 or 5 element layers, and the lower mantle 5 element layers, see Table 2 for an overview. Material parameters density, shear modulus and Young's modulus are volume-averaged values derived from the Preliminary Reference Earth Model (PREM; Dziewonski, Anderson 1981).

Previous studies (Brandes *et al.* 2012, 2015, 2018; Steffen *et al.* 2014b) have shown that the Earth model composition affects the timing of possible seismic activity. We therefore test a variety of Earth models (Table 3). The parameters represent commonly used Earth models on a global scale and dedicated models for northern Europe (Kierulf *et al.* 2014; Lambeck *et al.* 2010; Peltier *et al.* 2015; Steffen, Wu 2011). We thereby consider models with thinner (Lambeck *et al.* 2010; Peltier *et al.* 2015) and thicker (Kierulf *et al.* 2014) lithospheric thicknesses as well as softer (Peltier *et al.* 2015) and harder (Lambeck *et al.* 2010) lower mantle viscosity that are discussed in the literature. We also test models with lateral heterogeneities in either lithospheric thickness or mantle viscosity: Wang, Wu (2006) presented a global model of lithospheric thickness which we implement, see Brandes *et al.* (2018), for more information. Becker, Boschi (2002) provided the global seismic tomography model SMEAN, whereas we use the update SMEAN2 from 2016, which is converted to viscosity variations following Steffen *et al*. (2006) and Wu *et al.* (2013).

We test three different data-constrained ice chronologies as the load for the Earth models. The first is the commonly used global model ICE-6G by Peltier *et al.* (2015), version ICE-6G_C, at a spatial resolution of 0.5 × 0.5 degrees. The model has 500-year time steps from 26 ka BP to today. We use the North-European part of this model and add another sawtooth-type glaciation cycle from 216 to 126 (full load) to 116 ka BP (load-free) to increase result accuracy (Johnston, Lambeck 1999), and then crudely increase the load linearly until 26 ka BP. The second ice history model ANU-ICE is a combination of two regional ANU-ICE ice history models for the British Isles (Lambeck 1995; spatial resolution 0.125 × 0.25 degrees) and Fennoscandia together with the Barents and Kara seas (Lambeck *et al.* 2010; spatial resolution 0.25 × 0.5 degrees). This model spans two glaciation cycles from 240 ka BP to today. Time steps vary between 3 and 45 000 years. The third ice history model is the European part (Fennoscandia, the Barents/Kara seas and the British Isles) of GLAC (Tarasov *et al.* 2012; Tarasov 2013; Root *et al.* 2015; Nordman *et al.* 2015), model number 71340, at a spatial resolution of 0.25 × 0.5 degrees. The ice model is implemented in the GIA model in 500 (during deglaciation) to 2000 years (during glaciation) time steps. For all three chronologies, corresponding ocean loading is not included, which according to Steffen *et al.*

Table 2 Vertical dimensions and subdivision of models with fixed lithospheric thickness

Layer	Thickness [km]	Depth [km]	
1	5	5	Lithosphere
2	5	10	
3	5	15	
4	5	20	
5	5	25	
6	5	30	
7	30	60	
8	30	90	
9	30/50/70	120/140/160	Lithosphere or upper mantle
10	90/110/130	250	Upper mantle
11	170	420	
12	151	571	
13	100	671	
14	329	1000	Lower mantle
15	330	1330	
16	500	1830	
17	500	2330	
18	561	2891	

Table 3 Summary of tested Earth models. Model names are abbreviated forms of lithosphere and mantle parameters. Lat. Hetero. = laterally heterogeneous. WW6 = lithosphere model by Wang, Wu (2006). SMEAN2 = 2016 update of seismic tomography model SMEAN by Becker, Boschi (2002) converted into 3D mantle viscosity variations

Earth model name	Lithospheric thickness [km]	Upper-mantle viscosity (10^{20} Pa s)	Lower-mantle viscosity (10^{21} Pa s)
L090_ U520_L221	90	5	2
L090_ U520_L222	90	5	20
L120_SMEAN2	120	Lat. Hetero. (SMEAN2)	Lat. Hetero. (SMEAN2)
L140_ U520_L221	140	5	2
L140_ U520_L222	140	5	20
L160_SMEAN2	160	Lat. Hetero. (SMEAN2)	Lat. Hetero. (SMEAN2)
LTTZ_U520_L221	Lat. Hetero. (WW6)	5	2
LTTZ_U520_L222	Lat. Hetero. (WW6)	5	20

(2006) can affect the quantities, i.e. near the coasts in Fennoscandia, by about one order of magnitude of the signal. This uncertainty is well accommodated by the signal spread of tested earth and ice models.

The potential of triggering earthquake activity at a certain location is tested by calculating and analysing δCFS (see Brandes *et al.* 2015, for details). The δCFS represents the minimum stress required to reach faulting in a certain stress regime (compressional, neutral (strike-slip) or extensional). A negative δCFS value thereby indicates that the fault is stable, while a positive value means that GIA stress can induce faulting, e.g. so that the accumulated stress is temporarily released by an earthquake. For better visualization we add the zero line in Figs. 3–7 to indicate the threshold where such onset of fault motion is possible This separates each diagram into a zone of stability (below the zero line) and a zone of instability (above the zero line).

Although δCFS calculation is straightforward, there are many input parameter and assumptions that have to be made. For this study we assume the faults are optimally oriented. Thus, their strike and dip values promote faulting for a commonly used friction coefficient of 0.6 and faults are perpendicular to the maximum horizontal direction of the tectonic background stress. Inspection of the tectonic faults in Fig. 1 shows different fault orientations, and some are oriented in a nearly optimal sense, which supports our assumption. At the same time, the faults are assumed to be close to failure at the onset of glaciation which has been shown to be a reasonable assumption (Steffen *et al.* 2014a). This agrees with findings by Zoback, Townend (2001) and Zoback, Zoback (2015), who concluded that the intraplate crust is generally critically stressed and thus close to failure. Pore-fluid pressure is not investigated. The stress difference between maximum (S1) and minimum (S3) background stress is implemented in form of the R-value (stress ratio, Gephart, Forsyth 1984) and set to 0.5, which means that the average of minimum and maximum background stress is used for the intermediate stress S2. The δCFS is calculated for 12.5 km depth as our tests (not shown) yield only small depth-dependent differences that are within the spread of the Earth and ice models tested. The general δCFS behaviour (trends and turning points) is the same.

RESULTS

Figure 3 shows the δCFS at the 12 locations of Table 1 and Fig. 1 for the last 26,000 years if only ice model ICE-6G_C is used in combination with the 8 Earth models. At first, we consider a compressional background stress field which implies a thrust-faulting mechanism. A compressional background stress field is reasonable to assume based on the World Stress Map (Heidbach *et al.* 2018). During the LGM from ca. 26 to 19 ka BP (Clark *et al.* 2009), the δCFS is strongly negative, thus in the stability zone, at all locations. The δCFS spread between the different Earth models is ca. 1.0–1.5 MPa, whereas the models with thicker lithosphere of 120 km and larger are more negative. Between ca. 18 and 14 ka BP (location-dependent) δCFS strongly increases approaching or crossing the zero line, depending on the Earth model. In the Latvian locations 1–3, δCFS mainly crosses the zero line between 12 and 5 ka BP. At Rakuti (4) one model would reach the instability zone today. In the west-Lithuanian locations (5–8), the zero line is crossed earlier than in Latvia, at ca. 14 ka BP. After 5 ka BP, the δCFS of all Earth models is in the instability zone. The δCFS at the interior Lithuanian locations (9–11) as well as at Ryadino (12) in Russia reach instability earliest at ca. 15 ka BP. Choosing a different Earth model can move the zero-crossing close to today, e.g. at Liciškėnai (11). In general, Earth models with thinner lithosphere (90 km) reach instability earlier than those with thicker lithosphere or with lateral lithosphere thickness variations. The δCFS difference between all models today is less than 1 MPa.

As can be seen in Fig. 3, selecting Earth models L090_520_L221 and L160_SMEAN2 largely envelops the spread of tested models. Also, one can see that the δCFS behaviour in nearby locations is very similar, so we show the result for only one of the locations 1 and 2, 5–8, and 9–11, respectively. For clarity, we thus limit remaining analyses to those two Earth models, simply called 1D and 3D in the figures, and 6 different locations (1, 3, 4, 8, 10 and 12).

In Fig. 4, we also show δCFS results at those 6 locations for ice models ANU-ICE and GLAC. Clearly, both models yield different curves compared to ICE-6G_C. Maximum negative values during LGM reach more than 14 MPa and the increase thereafter is much steeper than for ICE-6G_C. Considering the 1D model, the zero line at Sārnate (1) is crossed with ANU-ICE 5000 years earlier than with ICE-6G_C. In turn, considering the 3D model, the zero line is crossed up to 2000 years later. Hence, possible onset of fault reactivation at Sārnate is suggested between 14–7 ka BP based on Figs. 3 and 4.

At Valmiera (3), the results with GLAC suggest a phase of possible GIA induced seismic activity 17–15 ka BP, then δCFS drops and may reach the instability threshold later again after deglaciation is completed. ANU-ICE 1D points to a possible short activity at 14 ka BP, then stable conditions until instability is reached again after deglaciation. Overall, fault reactivation at Valmiera could have been possible 17–15, 14, and after 9.5 ka BP based on our modelling results.

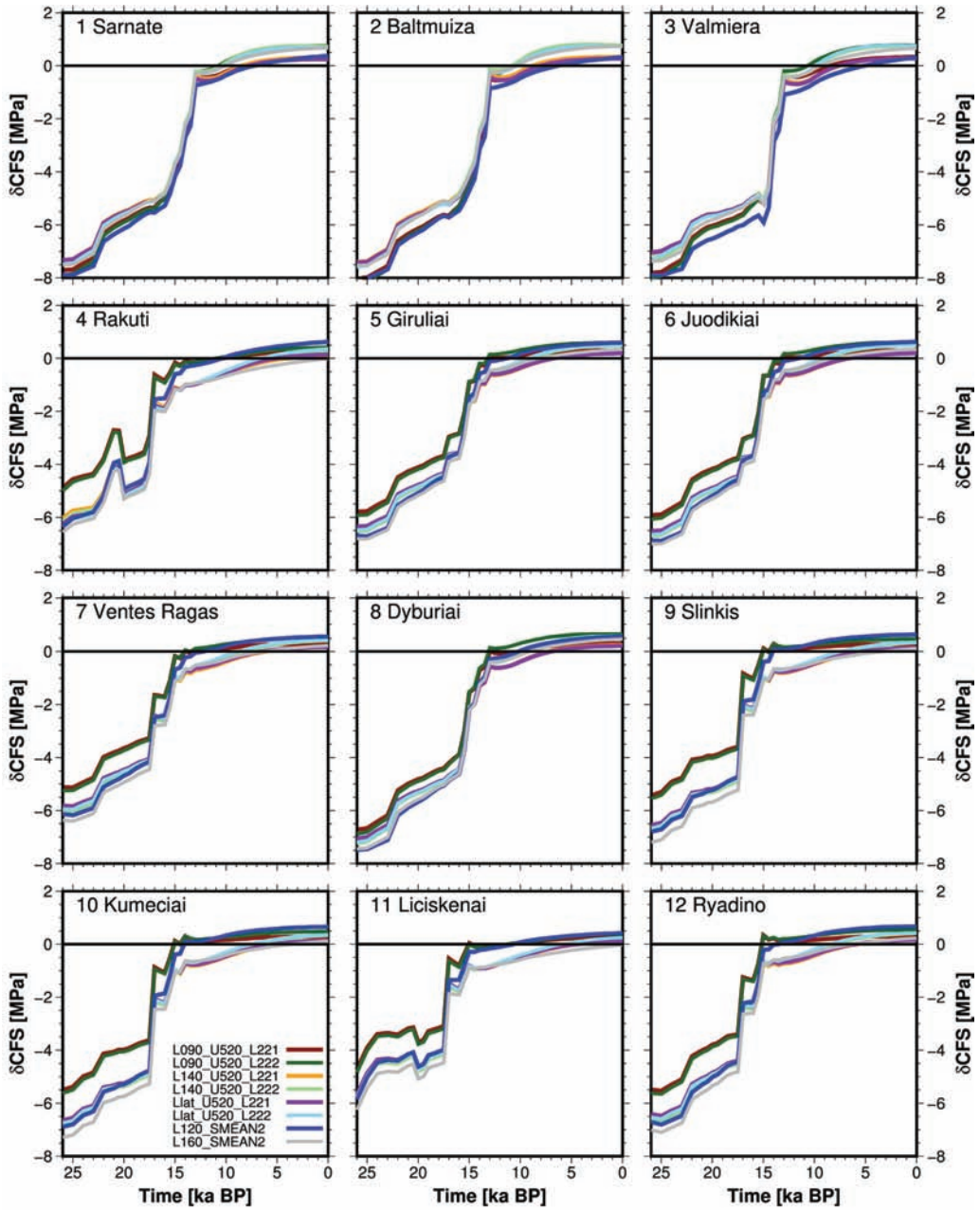

Fig. 3 Changes in Coulomb Failure Stress (δCFS) for thrust-faulting mechanism over time for the last 26 ka at the 12 locations shown in Fig. 1. ICE-6G_C (Peltier *et al.* 2015) is used as the ice load history model. The 8 curves of different colours represent the 8 rheology models listed in Table 1. δCFS is calculated at a depth of 12.5 km

At Rakuti (4), some models reach the instability zone after ca. 11.5 ka BP, while others may only reach them in the future. At Dyburiai (8), activity could happen earlier (ca. 15.5 ka BP) than based on results with ICE-6G_C only, while at Kumečiai (10) and Ryadino (12) timing is like that of ICE-6G_C. As for Rakuti, some δCFS curves of 3D models for Kumečiai do not cross the zero line but suggest it for the future. The GIA model spread after 12 ka BP is less than 2 MPa at all locations.

Some sediments in the SSDS horizons of the locations of Table 1 were dated to get insight into their possible time of generation. At Dyburiai, Kumečiai and Liciškėnai times much older than Late Weichselian were retrieved. We therefore show in Figs. 5 and 6 δCFS at 6 locations over the last 120,000 years to cover those times of possible activity. We only plot results for ANU-ICE and GLAC as ICE-6G_C is not available before LGM. At all locations, positive values are found from 120 ka BP (thus during Late Saalian times) until ca. 96 ka BP. Then, depending on the ice model, the zero line is touched or crossed at many different times until the Late Weichselian. The positive values are low and the gradients are rather flat before the zero line is reached. Any activity between ca. 60 and 50 ka BP at any of the locations can be excluded based on the modelling results.

The results so far assume a compressional back-

ground stress regime. Fig. 7 shows example results for an extensional (normal faulting, dotted) and neutral (strike-slip, dashed) background stress regime for all three tested ice models in combination with the 1D Earth model. In Lithuania and Russia as well as at the coastal locations of Latvia, fault reactivation can be excluded after 22 ka BP under normal faulting or strike-slip conditions. In Valmiera and Rakuti in Latvia, the instability threshold is reached (dependent on ice model) during LGM and a short period thereafter, but then stable conditions remain after 13–11 ka BP. At all locations, fault reactivation due to an extensional or neutral background stress regime is only found for the ANU-ICE and GLAC ice models, while it can be excluded if ICE-6G_C is applied.

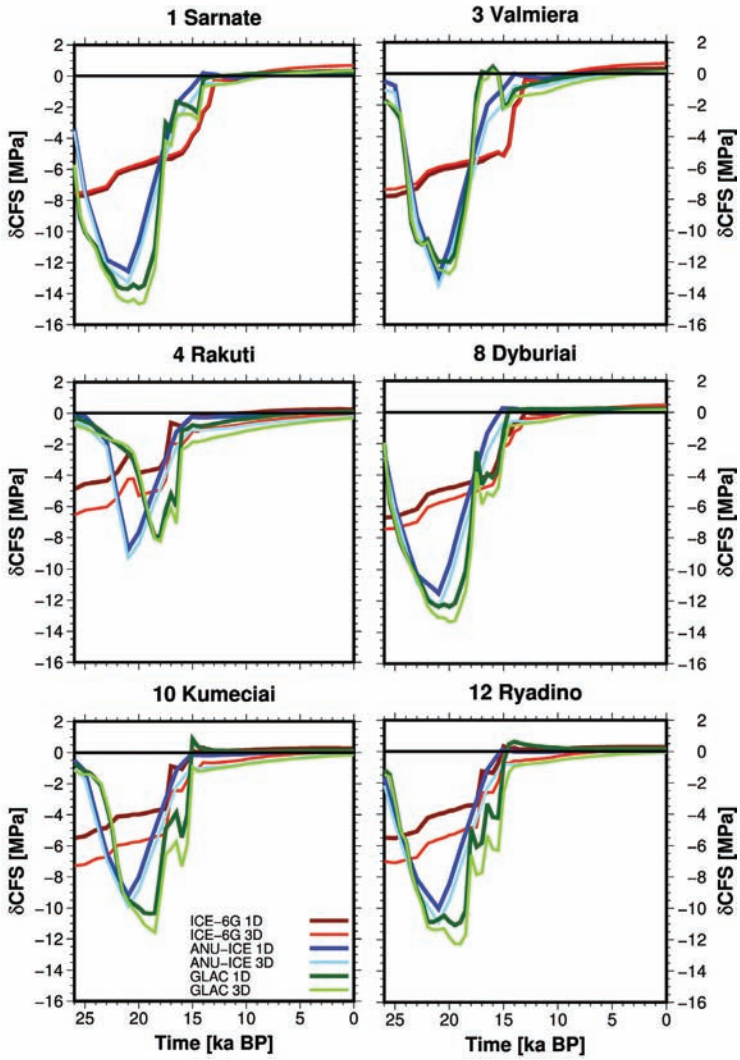

Fig. 4 Changes in Coulomb Failure Stress (δCFS) for thrust-faulting mechanism over time for the last 26 ka at 6 selected locations from Fig. 1. Next to ICE-6G_C (red, Peltier *et al.* 2015) also ANU-ICE (blue, Lambeck *et al.* 2010) and GLAC (green, Tarasov 2013) are used as ice load history models. The thicker, darker curves represent 1D Earth model L090_U520_L221 and the lighter, thinner curves 3D Earth model L160_SMEAN2, which both roughly envelope the curve spread in Fig. 3. δCFS is calculated at a depth of 12.5 km

DISCUSSION

Considering the generally accepted compressional background stress regime for our area under investigation, our results support the findings of glacially-induced seismites for the locations of Valmiera and Rakuti in Latvia as was suggested by van Loon *et al.* (2016). They suggested a deposition after 14.5 ka BP for Valmiera (Table 1) and our modelling can match this point in time with ANU-ICE (Fig. 4). Using GLAC or ICE-6-G_C times after 14.5 ka BP would also be possible, but mostly after 12 ka BP. GLAC also shows potential activity between ca. 17–15 ka BP. If an extensional background stress regime is assumed (Fig. 7), only GLAC would point to potential activity at exactly the time documented in van Loon *et al*. (2016). Hence, our different modelling results strongly support that SSDS at Valmiera are seismites due to glacially-induced seismicity. If a better dating of seismites would be achieved at Valmiera this may help in constraining our GIA models. Currently, ANU-ICE could be preferred but we note that we have made many assumptions whereas pore fluids can effectively alter the fault reactivation potential (Ranalli 1995), so that ICE-6G_C and GLAC model 71340 cannot be excluded yet.

Similarly, our models suggest activity at Rakuti after ca. 12 ka BP (Figs. 3 and 4). This does not match the findings of van Loon *et al.* (2016), who propose 17–16 ka BP. However, some models are very close to the zero line during that time, so we speculate that increased pore fluids, e.g. due to meltwater, could have acted as final trigger. Rakuti can therefore serve as a very crucial location to exclude some model configurations. Some models might be less preferable, if e.g. pore fluids are disregarded. For example, a model with thinner lithosphere of 90 km and either ice model ICE-6G_C or ANU-ICE would fit better than a 3D model with GLAC ice history. We note though that we have not tested other GLAC models which could potentially perform better.

Our results also support preliminary investigations of SSDS at Sārnate in Latvia (Nartišs *et al.* 2018) and Ryadino in Russia (Druzhinina *et al.* 2017), which could be glacially-induced seismites. Deposits at those locations cover a period of roughly 9–7 ka BP, which is well covered by many of our models independent of the chosen ice and Earth model combination (Figs. 3 and 4).

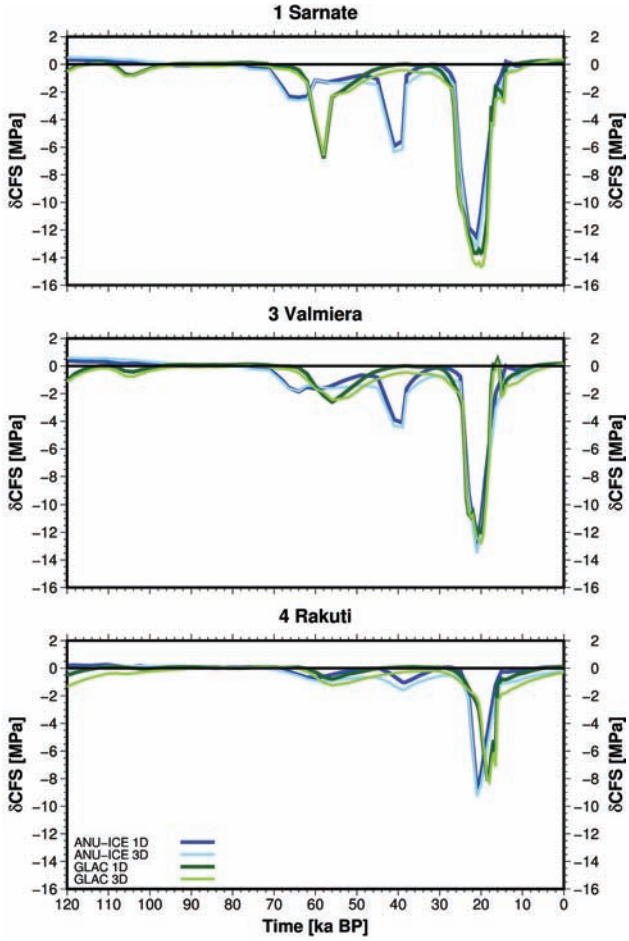

Fig. 5 Changes in Coulomb Failure Stress (δCFS) for thrust-faulting mechanism over time for the last 120 ka at 3 selected Latvian locations from Fig. 1 ANU-ICE (blue, Lambeck *et al.* 2010) and GLAC (green, Tarasov 2013) are only used as ice load history models as ICE-6G_C is not publicly available before the Last Glacial Maximum. The thicker, darker curves represent 1D Earth model L090_U520_L221 and the lighter, thinner curves 3D Earth model L160_SMEAN2, which both roughly envelope the curve spread in Fig. 3. δCFS is calculated at a depth of 12.5 km

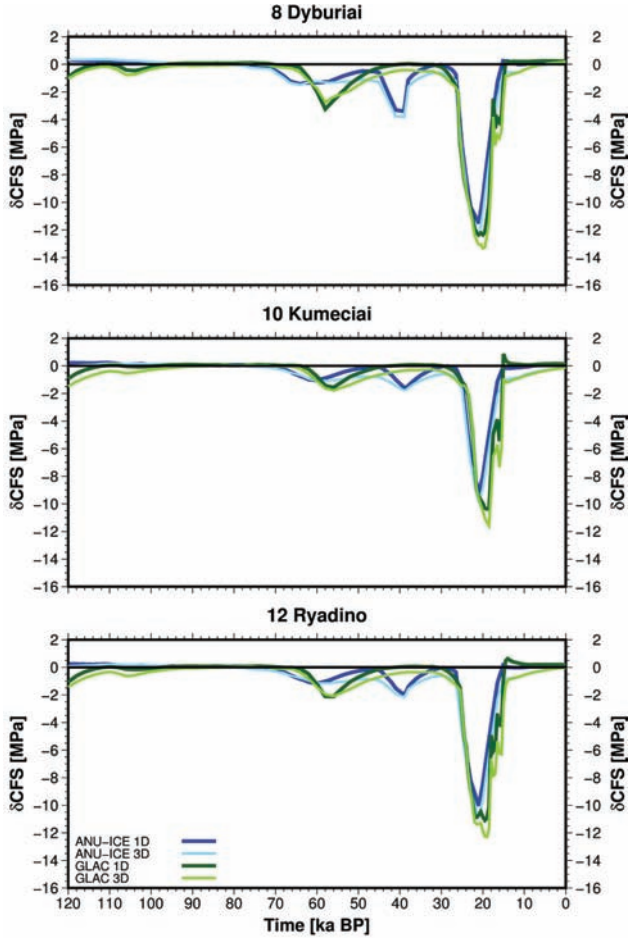

Fig. 6 As Fig. 5 but for two selected locations in Lithuania and one in the Kaliningrad District of Russia

At Baltmuiža, Belzyt *et al.* (2018a) provide deposition ages of 28.6–23.4 ka. There is no model that shows glacially-induced activity during this time (Figs. 3, 4 and 7). Moreover, the δCFS of most models is strongly negative so that we would exclude a glacial source of these SSDS.

The Giruliai mega-landslide likely happened 7.7 ka BP or thereafter (Bitinas *et al.* 2016; Damušytė, Bitinas 2018). All our modelled δCFS are past the instability threshold (Figs. 3 and 4) and thus a nearby fault could have been reactivated due to GIA. This could have triggered the earthquake that led to the mega-landslide. However, this remains very speculative and more research needs to be undertaken to find further evidence such as the presence of nearby faults and date-able seismites.

SSDS from Juodikiai and Ventės Ragas have yet to be dated and it is still unclear if these can be interpreted as seismites (Bitinas, Damušytė 2018). Our modelling suggests unstable conditions after 15 ka BP for those locations (Figs. 3 and 4). Both sediments are Late Weichselian in age and thus glacially-induced activity cannot be excluded. However, SSDS should be dated and investigated if they can be regarded as seismites.

In Dyburiai, dating of sediments points to a very early SSDS development between 119.7–91.1 ka BP which is possibly supported by our modelling results for both ANU-ICE and GLAC (Fig. 6). However, our models cannot limit the time span nor suggest a more certain point of seismic activity. We must also note that the δCFS is only slightly positive and small model adjustments could move the curves to stable conditions. In this regard, sophisticated geological investigations and dating could help in constraining the GIA models and exclude certain model setups.

At the Lithuanian locations of Slinkis, Kumečiai and Liciškėnai, we suggest other mechanisms as potential sources of the SSDS, as was discussed by Belzyt *et al.* (2018b); Pisarska-Jamroży *et al.* (2018c) and Woronko *et al.* (2018), respectively. During the times specified in Table 1, our models exhibit mainly

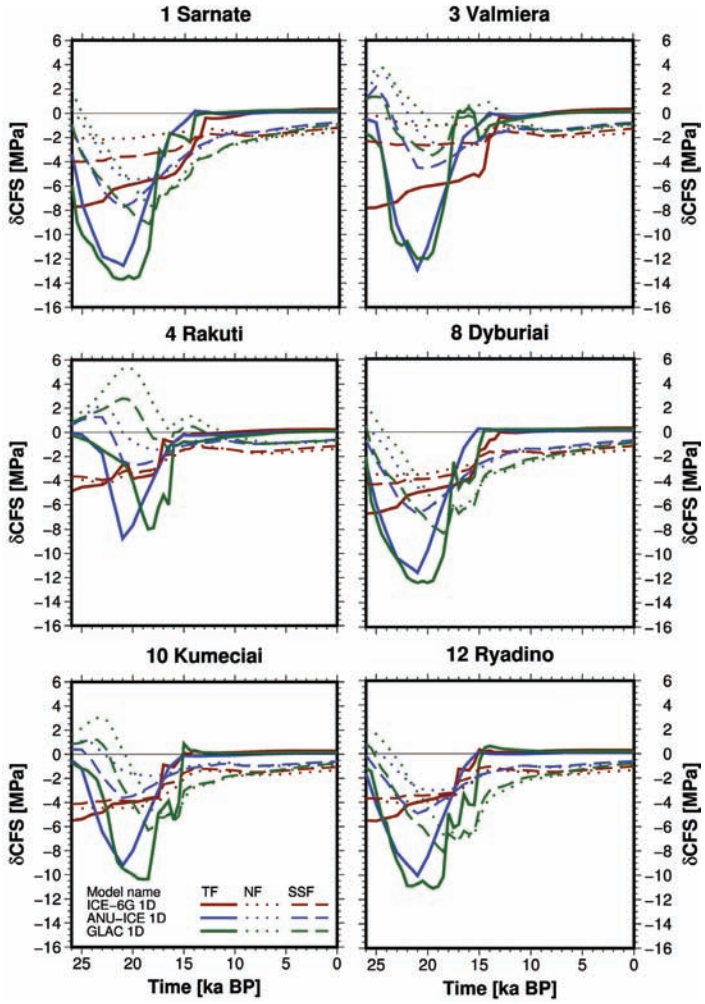

Fig. 7 Changes in Coulomb Failure Stress (δCFS) for thrust (solid), strike-slip (dashed) and normal (dotted) faulting mechanism over time for the last 26 ka at 6 selected locations from Fig. 1. The ice load history models are ICE-6G_C (red, Peltier *et al.* 2015), ANU-ICE (blue, Lambeck *et al*. 2010) and GLAC (green, Tarasov 2013). Only results for 1D Earth model L090_U520_L221 are shown. δCFS is calculated at a depth of 12.5 km

stable conditions (Figs. 3 and 6). For the location of Slinkis, this has interesting implications in view of the recent findings by Pisarska-Jamroży *et al.* (this issue), who suggest that "two well-defined layers with SSDS (dominated by water/sediment-escape structures and accompanying load structures) are linked to at least two phases of liquefaction processes, which may have been triggered by seismic shock derived from glacial isostatic earthquake or glacial earthquake". With our current model setup, we would exclude an earthquake due to GIA. However, if a glacial earthquake could also be excluded at Slinkis, this location can, as Rakuti in Latvia, serve as a very crucial location to exclude some model configurations.

Independent of the background stress field, all curves exhibit low gradients after 15–13 ka, with many in the instability zone or very close to the threshold, which results in a long interval where activity could be initiated. For some locations, several models cross the zero line around present day. Hence, GIA cannot be excluded as trigger of historic and quite recent earthquakes in the Baltic countries and the Kaliningrad District of Russia. Such connection has also been suggested for Germany and Denmark (Brandes *et al.* 2015, 2019).

Of course, these results are still subject to our used GIA models and assumptions made in the δCFS calculation. They may change if, for example, non-optimal faults or pore-fluid pressure are considered.

CONCLUSION

We have calculated δCFS at 12 selected locations in Latvia, Lithuania and the Kaliningrad District of Russia by applying a commonly used FE model of GIA. The locations are characterized by SSDS, which, if interpreted as seismites, indicate seismic activity. Previous and new preliminary geological studies suggest for some locations a possible connection of the SSDS formation to earthquakes that were likely triggered by lithospheric stress field changes induced by the decay of the Weichselian ice sheet. Within the stated assumptions of our study, our results show that all locations at several points in time have reached a state of fault instability, independent of the background stress regime and the chosen GIA model setup. Based on the dating of SSDS horizons, we cannot confirm GIA as source for certain SSDS locations, such as Slinkis, Kumečiai and Liciškėnai. At Sarnate, Valmiera, Rakuti, Dyburiai and Ryadino such relation is likely. In addition, the behaviour of δCFS curves after 15 ka BP suggests that historic and recent earthquakes in the East Baltic area (see e.g., Ņikuļins 2011; Pačėsa, Šliaupa 2011) could be an aftermath of the last glaciation which has already been considered for Germany and Denmark (Brandes *et al.* 2015, 2019).

The SSDS of Rakuti and Slinkis may serve as crucial locations to improve our GIA models as glacially-induced fault reactivation has been suggested from geological analysis (van Loon *et al*. 2016; Pisarska-Jamroży *et al*. this issue), but the GIA modelling cannot yet support this. If more SSDS are found and categorised as seismites, thorough dating of the deposition horizon can help in GIA modelling by excluding or supporting certain GIA model configurations. Locations of glacially-induced faulting can therefore serve next to relative sea levels, global positioning and gravimetric observations as additional constraint on GIA modelling.

ACKNOWLEDGMENTS

We are grateful for the constructive reviews of Willy Fjeldskaar and an anonymous reviewer as well as for additional remarks from the editor Albertas Bitinas that helped in improving the manuscript. We would like to thank Kurt Lambeck and Anthony Purcell for providing the ANU-ICE ice history and Valērijs Ņikuļins, Jurga Lazauskienė, Andrius Pačėsa and Saulius Šliaupa for providing the Latvian, Lithuanian and surrounding fault data, respectively, shown in Figure 1. We would also like to thank the participants of the International Palaeoseismological Field Workshop 2018 in Latvia and Lithuania for many fruitful discussions that initiated this study. All figures except Fig. 2 are drawn with GMT5 (Wessel *et al.* 2013). Rebekka Steffen acknowledges funding from the Swedish National Space Agency and the AXA Research Fund. This study is part of the GREBAL project (No. 2015/19/B/ST10/00661) from the National Science Centre Poland.

REFERENCES

ABAQUS 2018. *SIMULIA ABAQUS 2018 Documentation*. Dassault Systèmes.

Argus, D.F., Peltier, W., Drummond, R., Moore, A.W. 2014. The Antarctica component of postglacial rebound model ICE-6G_C (VM5a) based on GPS positioning, exposure age dating of ice thicknesses, and relative sea level histories. *Geophysical Journal International 198*, 537–563.

Becker, T.W., Boschi, L. 2002. A comparison of tomographic and geodynamic mantle models. *Geochemistry Geophysics Geosystems 3 (1)*, 2001GC000168.

Belzyt, S., Nartišs, M., Pisarska-Jamroży, M., Woronko, B., Bitinas, A. 2018a. Large-scale glaciotectonically-deformed Pleistocene sediments with deformed layers sandwiched between undeformed layers, Baltmuiža site, Western Latvia. In: Pisarska-Jamroży, M., Bitinas, A. (eds.) *Soft-sediment deformation structures and palaeoseismic phenomena in the South-eastern Baltic Region*. Excursion guide of International Palaeoseismological Field Workshop, 17–21st September 2018, Vilnius, Lithuania. Lithuanian Geological Survey, Lithuanian Geological Society, Vilnius, 38–42.

Belzyt, S., Pisarska-Jamroży, M., Bitinas, A., Damušytė, A., Woronko, B. 2018b. Soft-sediment deformation structures in the Pleistocene meandering-river floodplain (Slinkis outcrop, Central Lithuania). In: Pisarska-Jamroży, M., Bitinas, A. (eds.) *Soft-sediment deformation structures and palaeoseismic phenomena in the South-eastern Baltic Region*. Excursion guide of International Palaeoseismological Field Workshop, 17–21st September 2018, Vilnius, Lithuania. Lithuanian Geological Survey, Lithuanian Geological Society, Vilnius, 16–20.

Bitinas, A., Damušytė, A. 2018. Ventės Ragas outcrop and Juodikiai quarry: soft-sediment deformation structures of enigmatic genesis in the Lithuanian Maritime Region. In: Pisarska-Jamroży, M., Bitinas, A. (eds.) *Soft-sediment deformation structures and palaeoseismic phenomena in the South-eastern Baltic Region*. Excursion guide of International Palaeoseismological Field Workshop, 17–21st September 2018, Vilnius, Lithuania. Lithuanian Geological Survey, Lithuanian Geological Society, Vilnius, 26–30.

Bitinas, A., Lazauskienė, J. 2011. Implications of the palaeoseismic events based on the analysis of the structures of the Quaternary deposits. *Baltica* 24, Special Issue "Geosciences in Lithuania: challenges and perspectives", 127–130.

Bitinas A., Damušytė A., Vaikutienė G., 2016. Seisminiai reiškiniai pietryčių Baltijos kranto zonoje poledynmečiu. *Conference material to Jūros ir krantų tyrimai 2016: 9-oji mokslinė – praktinė konferencija, 27–29th April 2016, Klaipėda*, 27–31. (in Lithuanian).

Brandes, C., Winsemann, J., Roskosch, J., Meinsen, J., Tsukamoto, S., Frechen, M., Tanner, D.C., Steffen, H., Wu, P. 2012. Activity along the Osning Thrust in Central Europe during the Late glacial: ice-sheet and lithosphere interactions. *Quaternary Science Reviews 38*, 49–62.

Brandes, C., Steffen, H., Steffen, R., Wu, P. 2015. Intraplate seismicity in northern Central Europe is induced by the last glaciation. *Geology 43*, 611–614.

Brandes, C., Steffen, H., Sandersen, P.B.E., Wu, P., Winsemann, J. 2018. Glacially induced faulting along the NW segment of the Sorgenfrei-Tornquist Zone, northern Denmark: implications for neotectonics and Lateglacial fault-bound basin formation. *Quaternary Science Reviews 189*, 149–168.

Brandes C., Plenefisch T., Tanner D.T., Gestermann N., Steffen H. 2019. Evaluation of deep crustal earthquakes in northern Germany – Possible tectonic causes. *Terra Nova 31 (2)*, 83–93.

Clark, P.U., Dyke, A.S., Shakun, J.D., Carlson, A.E., Clark, J., Wohlfarth, B., Mitrovica, J.X., Hostetler, S.W., McCabe, A.M. 2009. The last glacial maximum. *Science 325 (5941)*, 710–714.

Cohen, K.M., Finney, S.C., Gibbard, P.L., Fan, J.-X. 2013 updated. The ICS International Chronostratigraphic Chart. *Episodes 36*, 199–204.

Čyžienė, J., Baliukevičius, A., Šliaupa, S., Lazauskienė, J. 2007. Lietuvos prekvartero stratonų struktūriniai žemėlapiai 1:200 000 masteliu (A set of Structural maps for the reference strata of the pre-Quaternary succession of Lithuania at a scale of 1:200 000). In: Satkūnas, J. (ed.) *Lietuvos Geologijos Tarnybos 2006 metų veiklos rezultatai (Lithuanian Geological Survey Annual Report 2006)*. Lithuanian Geological Survey, Vilnius, 30–32.

Damušytė, A., Bitinas, A. 2018. Giruliai mega-landslide (Litorina Sea palaeo-cliff): possible relict of palaeoseismic event. In: Pisarska-Jamroży, M., Bitinas, A. (eds.) *Soft-sediment deformation structures and palaeoseis-*

mic phenomena in the South-eastern Baltic Region. Excursion guide of International Palaeoseismological Field Workshop, 17–21st September 2018, Vilnius, Lithuania. Lithuanian Geological Survey, Lithuanian Geological Society, Vilnius, 31.

Doss, B. 1910. Die historisch beglaubigten Einsturzbeben und seismisch-akustischen Phänomene der russischen Ostseeprovinzen. *Gerlands Beitäge zur Geophysik 10*, 1–124.

Druzhinina, O., Bitinas, A., Molodkov A., Kolesnik, T. 2017. Palaeoseismic deformations in the Eastern Baltic region (Kaliningrad District of Russia). *Estonian Journal of Earth Sciences 66 (3),* 119–129.

Dziewonski, A.M., Anderson D.L. 1981. Preliminary reference Earth model. *Physics of the Earth and the Planetary Interiors 25*, 297–356.

Eaton, D.W., Darbyshire, F., Evans, R.L., Grütter, H., Jones, A.G., Yuan, X. 2009. The elusive lithosphere-asthenosphere boundary (LAB) beneath cratons. *Lithos 109*, 1–22.

Fenton, C. 1994. *Postglacial faulting in Eastern Canada*. Geological Survey of Canada Open File Report 2774, Natural Resources Canada, 94 pp.

Gephart, J.W., Forsyth, D.W. 1984. An improved method for determining the regional stress tensor using earthquake focal mechanism data: Application to the San Fernando Earthquake Sequence. *Journal of Geophysical Research 89*, 9305–9320.

Grube, A. 2019. Palaeoseismic structures in Quaternary sediments, related to an assumed fault zone north of the Permian Peissen-Gnutz salt structure (NW Germany) – Neotectonic activity and earthquakes from the Saalian to the Holocene. *Geomorphology 328*, 15–27.

Heidbach, O., Rajabi, M., Cui, X., Fuchs, K., Müller, B., Reinecker, J., Reiter, K., Tingay, M., Wenzel, F., Xie, F., Ziegler, M.O., Zoback, M.L., Zoback, M. 2018. The World Stress Map database release 2016: Crustal stress pattern across scales. *Tectonophysics 744*, 484–498.

Hoffmann, G., Reicherter, K. 2012. Soft-sediment deformation of late Pleistocene sediments along the southwestern coast of the Baltic Sea (NE Germany). *International Journal of Earth Sciences 101*, 351–363.

Johnston, P., Lambeck, K. 1999. Postglacial rebound and sea level contributions to changes in the geoid and the Earth's rotation axis. *Geophysical Journal International 136*, 537–558.

Kierulf, H.P., Steffen, H., Simpson, M.J.R., Lidberg, M., Wu, P., Wang, H. 2014. A GPS velocity field for Fennoscandia and a consistent comparison to glacial isostatic adjustment models. *Journal of Geophysical Research Solid Earth 119 (8)*, 6613–6629.

Lambeck, K. 1995. Late Devensian and Holocene shorelines of the British Isles and North Sea from models of glacio-hydro-isostatic rebound. *Journal of the Geological Society London 152*, 437–448.

Lambeck, K., Purcell, A., Zhao, J., Svensson, N.-O. 2010. The Scandinavian ice sheet: from MIS 4 to the end of the last glacial maximum. *Boreas 39 (2)*, 410–435.

Lambeck, K., Rouby, H., Purcell, A., Sun, Y., Sambridge, M. 2014. Sea level and global ice volumes from the Last Glacial Maximum to the Holocene. *Proceedings of the National Academy of Sciences of the United States of America 111 (43)*, 15296–15303.

Lund, B. 2015. Palaeoseismology of glaciated terrain. In: Beer, M., *et al*. (eds.). *Encyclopedia of Earthquake Engineering*. Springer-Verlag, Berlin, Heidelberg, 1765–1779.

Mikko, H., Smith, C.A., Lund, B., Ask, M.V.S., Munier, R. 2015. LiDAR-derived inventory of post-glacial fault scarps in Sweden. *GFF 137*, 334–338.

Nartišs, M., Woronko, B., Pisarska-Jamroży, M., Belzyt, S., Bitinas, A. 2018. Injection structures and load casts in lagoon sediments (Sārnate outcrop, W Latvia). In: Pisarska-Jamroży, M., Bitinas, A. (eds.) *Soft-sediment deformation structures and palaeoseismic phenomena in the South-eastern Baltic Region*. Excursion guide of International Palaeoseismological Field Workshop, 17–21st September 2018, Vilnius, Lithuania. Lithuanian Geological Survey, Lithuanian Geological Society, Vilnius, 32–37.

Ņikuļins, V. 2011. Assessment of the seismic hazard in Latvia. Version of 2007 year. *Scientific Journal of Riga Technical University 24*, 110–115.

Ņikuļins, V. 2019. Geodynamic Hazard Factors of Latvia: Experimental Data and Computational Analysis. *Baltic Journal of Modern Computing 7 (1)*, 151–170.

Nordman, M., Milne, G., Tarasov, L. 2015. Reappraisal of the Angerman River decay time estimate and its application to determine uncertainty in Earth viscosity structure. *Geophysical Journal International 201*, 811–822.

Pačėsa A., Šliaupa S. 2011. Seismic activity and seismic catalogue of the East Baltic region. *Geologija 53 (3(75))*, 134–146.

Peltier, W., Argus, D., Drummond, R. 2015. Space geodesy constrains ice age terminal deglaciation: The global ICE-6G_C (VM5a) model. *Journal of Geophysical Research Solid Earth 120*, 450–487.

Pisarska-Jamroży, M., Bitinas, A. 2018. *Soft-sediment deformation structures and palaeoseismic phenomena in the South-eastern Baltic Region*. Excursion guide of International Palaeoseismological Field Workshop, 17–21st September 2018, Vilnius, Lithuania. Lithuanian Geological Survey, Lithuanian Geological Society, Vilnius.

Pisarska-Jamroży, M., Belzyt, S., Börner, A., Hoffmann, G., Hüneke, H., Kenzler, M., Obst, K., Rother, H., van Loon, A.J. 2018a. Evidence from seismites for glacio-isostatically induced crustal faulting in front of an advancing land-ice mass (Rügen Island, SW Baltic Sea), *Tectonophysics 745*, 338–348.

Pisarska-Jamroży, M., Belzyt, S., Bitinas, A., Jusienė, A., Damušytė, A., Woronko, B. 2018b. A glaciolacustrine succession (Dyburiai outcrop, NW Lithuania) with numerous deformed layers sandwiched between undeformed layers. In: Pisarska-Jamroży, M., Bitinas, A. (eds.) *Soft-sediment deformation structures and palaeo-*

seismic phenomena in the South-eastern Baltic Region. Excursion guide of International Palaeoseismological Field Workshop, 17–21st September 2018, Vilnius, Lithuania. Lithuanian Geological Survey, Lithuanian Geological Society, Vilnius, 43–48.

Pisarska-Jamroży, M., Belzyt, S., Woronko, B., Bitinas, A., Damušytė, A. 2018c. Dozens of deformed layers sandwiched between undeformed layers in fluvial sediments (Kumečiai outcrop, Central Lithuania). In: Pisarska-Jamroży, M., Bitinas, A. (eds.) *Soft-sediment deformation structures and palaeoseismic phenomena in the South-eastern Baltic Region*. Excursion guide of International Palaeoseismological Field Workshop, 17–21st September 2018, Vilnius, Lithuania. Lithuanian Geological Survey, Lithuanian Geological Society, Vilnius, 21–25.

Pisarska-Jamroży, M., Belzyt, S., Bitinas, A., Jusienė, A. Woronko, B., this issue. Seismic shocks, periglacial conditions and glacitectonics as causes of the deformation of a Pleistocene meandering river succession in central Lithuania. *Baltica*, this issue.

Ranalli, G. 1995. *Rheology of the Earth*. Chapman & Hall, London, 414 pp.

Root, B.C., Tarasov, L., van der Wal, W. 2015. GRACE gravity observations constrain Weichselian ice thickness in the Barents Sea. *Geophysical Research Letters 42*, 3313–3320.

Sandersen, P.B.E., Jørgensen, F. 2015. Neotectonic deformation of a Late Weichselian outwash plain by deglaciation-induced fault reactivation of a deep-seated graben structure. *Boreas 44*, 413–431.

Sharov, N.V., Malovichko, A.A., Schukin, Y.K. 2007. The Earthquakes and Microseismicity in the Problems of Contemporary Geodynamics of the East European Platform. Book 1 Earthquakes. Petrozavodsk: KarNC RAN, 381 pp. (in Russian).

Spada, G., Barletta, V.R., Klemann, V., Riva, R.E.M., Martinec, Z., Gasperini, P., Lund, B.,Wolf, D., Vermeersen, L.L.A., King, M.A. 2011. A benchmark study for glacial isostatic adjustment codes. *Geophysical Journal International 185*, 106–132.

Steffen, H., Wu, P. 2011. Glacial isostatic adjustment in Fennoscandia – A review of data and modeling. *Journal of Geodynamics 52*, 169–204.

Steffen, H., Kaufmann, G., Wu, P. 2006. Three-dimensional finite-element modeling of the glacial isostatic adjustment in Fennoscandia. *Earth Planetary Science Letters 250*, 358–375.

Steffen, R., Steffen, H., Wu, P., Eaton, D.W. 2014a. Stress and fault parameters affecting fault slip magnitude and activation time during a glacial cycle. *Tectonics 33*, 1461–1476.

Steffen, R., Wu, P., Steffen, H., Eaton, D.W. 2014b. The effect of earth rheology and ice-sheet size on fault slip and magnitude of postglacial earthquakes. *Earth Planetary Science Letters 388*, 71–80.

Steffen, R., Steffen, H., Wu, P., Eaton, D.W. 2015. Reply to comment by Hampel *et al*. on "Stress and fault parameters affecting fault slip magnitude and activation time during a glacial cycle". *Tectonics 34*.

Stewart, I.S., Sauber, J., Rose, J. 2000. Glacio-seismotectonics: ice sheets, crustal deformation and seismicity. *Quaternary Science Reviews 19 (14–15)*, 1367–1389.

Stewart, I.S., Firth, C.R., Rust, D.J., Collins, P.E.F., Firth, J.A. 2001. Postglacial fault movement and palaeoseismicity in western Scotland: A reappraisal of the Kinloch Hourn fault, Kintail. *Journal of Seismology 5*, 307–328.

Tarasov, L. 2013. GLAC-1b: A new data-constrained global deglacial ice sheet reconstruction from glaciological modelling and the challenge of missing ice. *Geophysical Research Abstracts 15*, EGU2013-12342.

Tarasov, L., Dyke, A.S., Neal, R.M., Peltier, W.R. 2012. A data-calibrated distribution of deglacial chronologies for the North American ice complex from glaciological modelling, *Earth Planetary Science Letters 315*, 30–40.

Ulomov, V.I., Akatova, K.N., Medvedeva, N.S. 2008. Estimation of Seismic Hazard in the Kaliningrad Region. *Izvestiya, Physics of the Solid Earth 44 (9)*, 691–705.

van Loon, A.J., Pisarska-Jamroży, M. 2014. Sedimentological evidence of Pleistocene earthquakes in NW Poland induced by glacio-isostatic rebound. *Sedimentary Geology 300*, 1–10.

van Loon, A.J., Pisarska-Jamroży, M., Nartiss, M., Krievans, M., Soms, J. 2016. Seismites resulting from high-frequency, high-magnitude earthquakes in Latvia caused by Late Glacial glacio-isostatic uplift. *Journal of Palaeogeography 5*, 363–380.

Wang, H., Wu, P. 2006. Effects of lateral variations in lithospheric thickness and mantle viscosity on glacially induced relative sea levels and long wavelength gravity field in a spherical, self-gravitating Maxwell Earth. *Earth Planetary Science Letters 249 (3)*, 368–383.

Wessel, P., Smith, W.H.F., Scharroo, R., Luis, J.F., Wobbe, F. 2013. Generic Mapping Tools: Improved version released. *EOS Transactions American Geophysical Union 94*, 409–410.

Whitehouse, P.L. 2018. Glacial isostatic adjustment modelling: historical perspectives, recent advances, and future directions. *Earth Surface Dynamics 6*, 401–429.

Woronko, B., Pisarska-Jamroży, M., Belzyt, S., Karmazienė, D., Bitinas, A., Damušytė, A. 2018. Multi-type soft-sediment deformation structures in glaciolacustrine kame sediments (Liciškėnai outcrop, S Lithuania). In: Pisarska-Jamroży, M., Bitinas, A. (eds.) *Soft-sediment deformation structures and palaeoseismic phenomena in the South-eastern Baltic Region*. Excursion guide of International Palaeoseismological Field Workshop, 17–21st September 2018, Vilnius, Lithuania. Lithuanian Geological Survey, Lithuanian Geological Society, Vilnius, 10–15.

Wu, P. 1992. Viscoelastic versus viscous deformation and the advection of pre-stress. *Geophysical Journal International 108*, 136–142.

Wu, P. 2004. Using commercial finite element packages

for the study of earth deformations, sea levels and the state of stress. *Geophysical Journal International 158*, 401–408.

Wu, P., Johnston, P. 1998. Validity of using flat-earth finite element models in the study of postglacial rebound. In: P. Wu (ed.). *Dynamics of the Ice Age Earth: a Modern Perspective*. Trans Tech Pub., Zürich, Switzerland, 191–202.

Wu, P., Wang, H., Steffen, H. 2013. The role of thermal effect on mantle seismic anomalies under Laurentia and Fennoscandia from observations of glacial isostatic adjustment. *Geophysical Journal International 192*, 7–17.

Zoback, M.D., Townend, J. 2001. Implications of hydrostatic pore pressures and high crustal strength for the deformation of intraplate lithosphere. *Tectonophysics 336*, 19–30.

Zoback, M.L., Zoback, M. 2015. Lithosphere Stress and Deformation. *Treatise on Geophysics 6*.